Real time simulation of organ motions induced by breathing: first evaluation on patient data.

A. Hostettler[1], S.A. Nicolau[1], C. Forest[1], L. Soler[1], Y. Remond[2]

[1] IRCAD-Hopital Civil, Virtual-surg, 1 Place de l'Hopital, 67091 Strasbourg Cedex
{alexandre.hostettler, luc.soler}@ircad.u-strasbg.fr
[2] Institut de Mécanique des Fluides et des Solides, 2 rue Boussingault 67000 Strasbourg

Abstract. In this paper we present a new method to predict in real time from a preoperative CT image the internal organ motions of a patient induced by his breathing. This method only needs the segmentation of the bones, viscera and lungs in the preoperative image and a tracking of the patient skin motion. Prediction of internal organ motions is very important for radiotherapy since it can allow to reduce the healthy tissue irradiation. Moreover, guiding system for punctures in interventional radiology would reduce significantly their guidance inaccuracy. In a first part, we analyse physically the breathing motion and show that it is possible to predict internal organ motions from the abdominal skin position. Then, we propose an original method to compute from the skin position a deformation field to the internal organs that takes mechanical properties of the breathing into account. Finally, we show on human data that our simulation model can provide a prediction of several organ positions (liver, kidneys, lungs) at 14 Hz with an accuracy within 7 mm.

1 Introduction

Preoperative 3D CT images are used in many medical contexts. For some of them, the breathing motion is an issue that is taken into account but not compensated. For instance, in radiotherapy the dosimetry computation is performed on a static preoperative CT image although the patient breathes freely during the irradiation. Then, the planned volume targeting is overestimated so as to totally irradiate the tumour. Consequently, healthy tissue irradiations are much more important than if the tumour position was perfectly known during the breathing. In interventional radiology, guiding systems for punctures provide a limited accuracy since the breathing movements are not compensated [10, 16].

Respiratory gating techniques [11, 17, 2] are a first attempt to reduce the breathing influence. The patient is immobilized on the intervention table and his breathing is monitored to synchronize his lung volume to the one during the preoperative CT acquisition. These methods are however constraining: they lengthen the intervention, they are uncomfortable for the patient and the repositioning accuracy, of 1.5 mm on average, can sometimes exceed 5 mm [2].

Therefore, a predictive method to simulate the abdomen and thorax breathing motions would be a great improvement for the previous reported applications. Internal motion during a quiet breathing being between 10 and 25 mm [4], practitioners estimate that a prediction accuracy within 4 mm would bring a significant improvement to the current protocol in radiotherapy and interventional radiology.

Solutions to simulate organ mesh deformations and interactions are numerous [5, 7, 15, 8], however they require the rheological parameters of the patient organs to provide predictive results, which is currently an unsolved issue. Consequently, these methods that were developed for realistic simulation of surgical interventions, are not adapted to intra-operative applications in the operating room.

Sarrut et al. propose to simulate an artificial 3D+t CT image during a breathing cycle from two CT images acquired at inhale and exhale breath-hold. Simulated 3D+t images are built by a vector field interpolation between both CT images [12]. Although this interesting method provides a simulated CT image in real time, it implies a supplementary irradiation of the patient since it requires at least two CT acquisitions whereas only one is done routinely. Moreover, it assumes that the breathing is perfectly reproducible and cyclical. Therefore, this method is limited to patients who are under general anesthesia and intubated.

In this paper we present a new method to provide in real time 3D CT or mesh images that simulate the patient breathing from a single pre-operative CT acquisition. In Sec. 2, we firstly describe qualitatively the breathing motion and show that an estimation of the internal organ position can be obtained from the skin position. In Sec. 3, we propose a method to compute from the skin position a deformation field applied to the internal organs. Finally, we provide in Sec. 4 a first evaluation of our method on human data showing that our simulation can be computed at 14 Hz with a prediction accuracy between 5 and 7 mm.

2 Estimation of the organ deformation from the skin position

Breathing movements are mainly caused by two sets of muscles: the intercostal muscles and the diaphragm. Those muscles move the thorax and the abdomen. Firstly, intercostal muscles induce the rib rotation around the vertebrae that makes the thorax volume change (cf. Fig. 1). This bone rotation is made possible since the sternum is linked to the ribs through deformable cartilage. Secondly, the diaphragm contraction dilates the lungs, causing the air insufflation. During a contraction, the diaphragm moves down and compresses the viscera, increasing the abdomen volume since most of the internal organs are incompressible and since viscera movements toward the feet is limited by the pelvis. Note that the abdominal muscles, the sterno cleido mastoidien, the scalene muscles, the trapeze muscles, the major dorsal muscles and the major pectoral muscle are involved as well in the breathing movements. However, they can be neglected in our context since they are essentially used during an important physical activity.

This qualitative description of the breathing motion highlights the link between skin and internal organ positions. Indeed, from the skin position, we can understand how the viscera are compressed, and then the diaphragm position and the lung volume. Therefore, we think that it is possible to estimate the internal organ motion from skin position. Consequently, we consider in our model that the patient inspiration increases the lung volume (and the thorax volume) and pushes the viscera down, which increases the abdomen volume. We assume that the volume of the viscera [13] and that the tissue thickness between skin and organs remain constant (cf. Fig. 1). In addition, we suppose that the viscera have homogeneous mechanical properties.

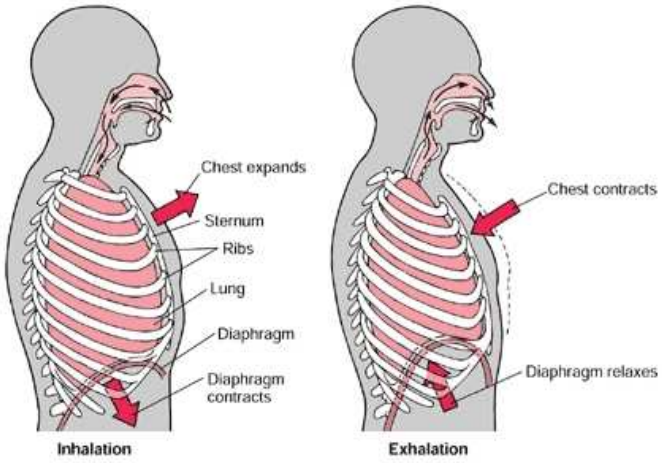

Fig. 1. Qualitative description of breathing. During the breathing, the bone rotation around the vertebrae makes the thorax volume change, and the diaphragm contraction compresses the viscera, causing the abdominal volume increase.

3 Simulation methodology

3.1 Set up

Our goal is to provide in real time a 3D deformation field to be applied on a preoperative CT or on the surfacic organ meshes previously extracted from the preoperative CT during a segmentation step. This deformation field is computed from the skin movements that are tracked in real time by an external system. In our set up, the patient is lying on the table (CT or radiotherapy table) and a tracking system provides in real time either a surface reconstruction of his abdominal and thoracic skin or feature points (for instance, some radio-opaque markers stuck on the patient skin before the preoperative CT acquisition). The registration between the CT frame and the tracking system frame is done using either the surfacic skin reconstruction or the feature points. We recall our method needs a segmentation of the 3D CT image into four different zones: skin, bones, lungs and viscera (liver, kidney, spleen, etc.): several software provide efficient

tools to perform a quick and accurate organ segmentation [3, 14]. In the following we call *internal envelope* the envelope of the lungs and the viscera.

In this section, firstly we explain how the skin, the bones and the internal envelope meshes are computed from the skin position. Secondly, we detail how we generate a deformation field from the internal envelope movement. In the following, we assume that the skin position is tracked using radio-opaque markers uniformly stuck on the patient skin.

3.2 Skin, bones and sternum

The displacement $\overrightarrow{D}$ of any point P of the surfacic skin mesh is computed from the displacements $\overrightarrow{V}_1, \overrightarrow{V}_2, \overrightarrow{V}_3, \overrightarrow{V}_4$ of the four closest markers M_1, M_2, M_3, M_4 with the following formula:

$$\overrightarrow{D} = k \cdot \frac{\sum_{i=1}^{4} 1/d_i \cdot \overrightarrow{V}_i}{\sum_{i=1}^{4} 1/d_i} \quad \text{with} \quad k = \frac{\sum_{i=1}^{4} 1/d_i \cdot \| \overrightarrow{V}_i \|}{\sum_{i=1}^{4} 1/d_i}$$

where d_i is the distance between M_i and P.

The rib movement is modelled by a rotation around the vertebra. We assume that the distance between sternum and skin remains constant and that the sternum is attached to the fourth rib pair. We choose the fourth pair since it minimizes the cartilage impact. Note that the simulation of the rib movement has no impact on the volume computation but only on the realism of rib and sternum position.

3.3 Movement of internal envelope

We call *internal organs* the union of lungs and viscera. To determine the movement of those organs we first study the movement of their envelope. This *internal envelope* is a convex balloon localized inside the trunk volume (cf. Fig 2). The movement of that balloon is computed in a way similar to the one that was used for the skin (cf. Fig 3): for each vertex, we look for the three closest skin markers and the resulting vertex displacement is computed from the displacements of these markers. Note that this method keeps a constant thickness between the internal envelope and skin.

The viscera go down along a curved axis that corresponds to the gravity centre of the viscera in each slice, filling the current volume of the computed internal envelope from the pelvis to the diaphragm. By hypothesis, viscera are incompressible, therefore a modification of the CT slice surface results in a change in the slice thickness. For the lungs, the slice thickness is uniformly changed to fill the remaining volume of the internal envelope (cf. Fig 2).

3.4 Generation of the deformation field

To describe the movement of each point in the internal envelope, we propose the following method to generate a deformation field. In each slice of the internal

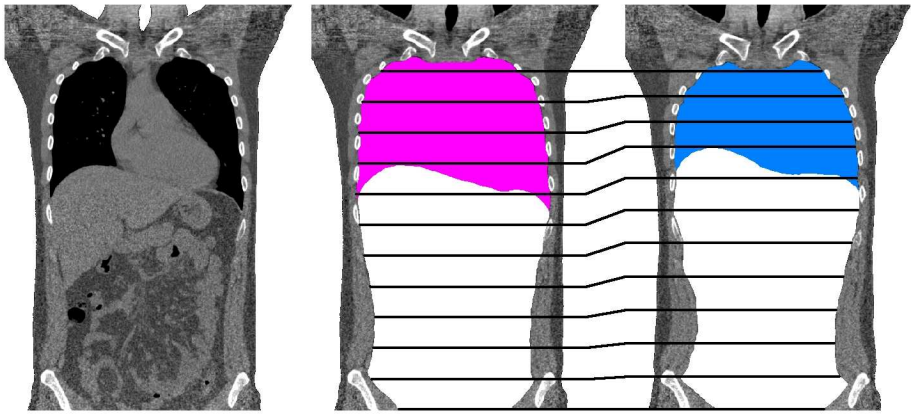

Fig. 2. Left: sagital slice of a patient showing the lungs and the viscera. The *internal envelope* is the convex balloon that contains the lung and the viscera. They are segmented in homogeneous grey and white on the middle image (inspiration phase). Since most of the internal organs are incompressible and since viscera movements toward the feet is limited by pelvis, we modify the thickness of each CT slice of the preoperative CT to keep its own volume constant (right image). The black lines represent the position of several corresponding CT slices from the inspired CT image on left, and the simulated expired image on right.

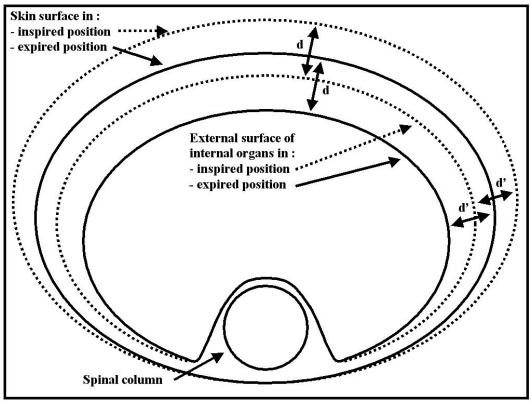

Fig. 3. The motion of the *internal envelope* is computed from the motion of the skin. Indeed, tissues contained between the skin and the internal envelope are almost incompressible, then the thickness between them remains constant.

envelope, the perimeter is divided into segments of identical size, allowing to control the internal deformation of that slice in an homogeneous way (cf. Fig. 4). For each point P we want to displace, we look for the two nearest vertices of

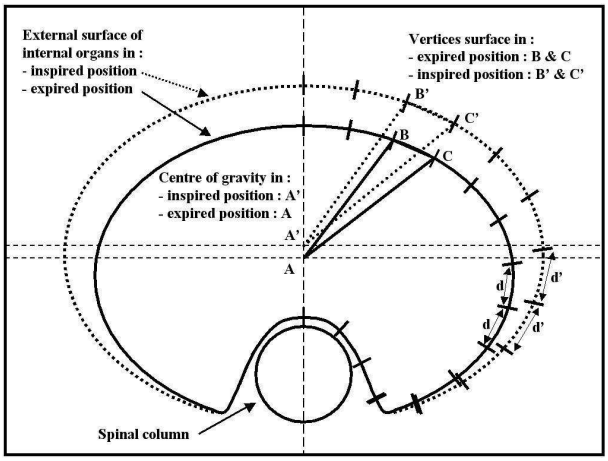

Fig. 4. Deformation field generation. In each slice of the internal envelope, the perimeter is divided into segments of identical size, and the gravity center is computed. Then, the displacement of a point is computed as a linear interpolation of the movement of the two nearest points of the perimeter (B and C) and the gravity center (A).

the envelope B and C, and to the nearest vertex of the mean barycentric axis A. The displacement is then computed with the interpolation formula used for the skin (see Sec. 3.2). This allows to easily animate 3D meshes in real-time. Animating a CT image is trickier as we do not want to know the destination of each pixel, but its provenance. In this case, the reverse application is computed and applied on each point of the 3D CT image.

4 First evaluation on human data

In order to evaluate the computation time needed by our simulation model and its prediction accuracy, we use the data of a human volunteer. Thirty radio-opaque markers have been stuck on his skin (cf. figure 5) and two CT acquisitions were performed in inspiration and expiration positions. Then, the voluntary remained lying on the table and a stereoscopic video tracking of the markers (tracking accuracy < 0.5 mm) was performed during 100 breathing cycles and recorded (see [9] for the used tracking method). The segmentation step (lungs, bones, viscera and radio-opaque markers) was performed by our medical staff for both CT acquisitions.

4.1 A real time simulation method

To register the expired CT image in the tracking system frame, we used the radio-opaque markers segmented in the CT image and performed a 3D/3D registration [1] with the marker set, among all the one recorded by our tracking system, that minimized the RMS registration error (1.1 mm for this case). Then, we measured

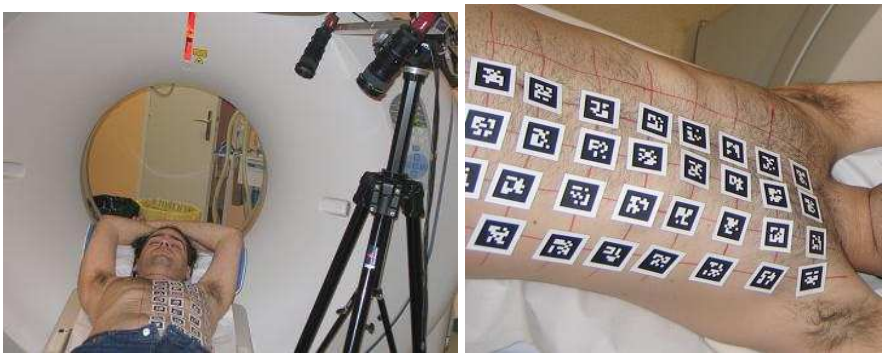

Fig. 5. Set up for the human data acquisition. Thirty markers have been stuck on the volunteer skin, then a stereoscopic video tracking of the markers is performed during 100 breathing cycles and recorded. ARTag markers were used [6]

the time needed to compute and display the simulated mesh and predicted CT image for the marker positions recorded during the voluntareer's breathing. Our simulation reached a frame rate around 14 Hz on a standard PC (2 GHz, 1Go RAM) with no implemented code optimization.

4.2 An accurate prediction

To evaluate the prediction accuracy, we used the inspired CT as the preoperative CT data from which the simulation is computed. Then, we computed the skin marker excursions from the inspired position to the expired position (extracted from the second CT image) and finally computed the deformation field. Therefore, a comparison of the simulated positions of the skin and internal organs with their true positions in the expired CT image is possible.

Qualitative results are visible in Fig. 6. To evaluate quantitatively the discrepancy between each simulated S and true T organ, we computed for each organ the average distance between one mesh vertex and its closest neighbour in the other mesh:

$$\epsilon = \text{mean}_{i \in S}(\parallel \text{mesh}_S(i) - \textit{closest point}(\text{mesh}_T(i)) \parallel)$$

We compute as well the same error for a distance under and above 3 mm:

$$\epsilon_1 = \text{mean}_{i \in S}(\parallel \text{mesh}_S(i) - \textit{closest point}(\text{mesh}_T(i)) \parallel > 3mm)$$

$$\epsilon_2 = \text{mean}_{i \in S}(\parallel \text{mesh}_S(i) - \textit{closest point}(\text{mesh}_T(i)) \parallel < 3mm)$$

This 3 mm threshold was chosen since we observed that the main prediction error of our model is along specific deformation axis. Without this threshold, this error is about 3 mm for the kidney for instance. This does not significantly point out the deformation error at its top and bottom, since it is averaged by the longitudinal points of the two meshes that are very close. Tab. 1 reports

the prediction error for kidney, liver, lungs and skin. We add into bracket the percentage of vertex for which the distance is above 3 mm. Note that pancreas, stomach, and spleen are not reported since they could not be segmented in the CT images. Indeed, to limit the irradiation undergone by the voluntary, the CT image was done with a low mA value (under 30 mA whereas a standard image is done with 70 mA) and without contrast agent. Therefore, the CT image was of insufficient quality to allow an accurate segmentation of these organs.

	Left kidney	Right kidney	Liver	Lungs	Skin
Total error ϵ in mm	3.4	3.7	3.7	3.3	1.0
error ϵ_1 in mm (>3mm)	5.5 (51 %)	6.0 (51 %)	6.3 (48 %)	6.5 (39 %)	2.4 (32 %)
error ϵ_2 in mm (<3mm)	1.4	1.5	1.3	1.2	0.4

Table 1. Results of the system evaluation on three patients.

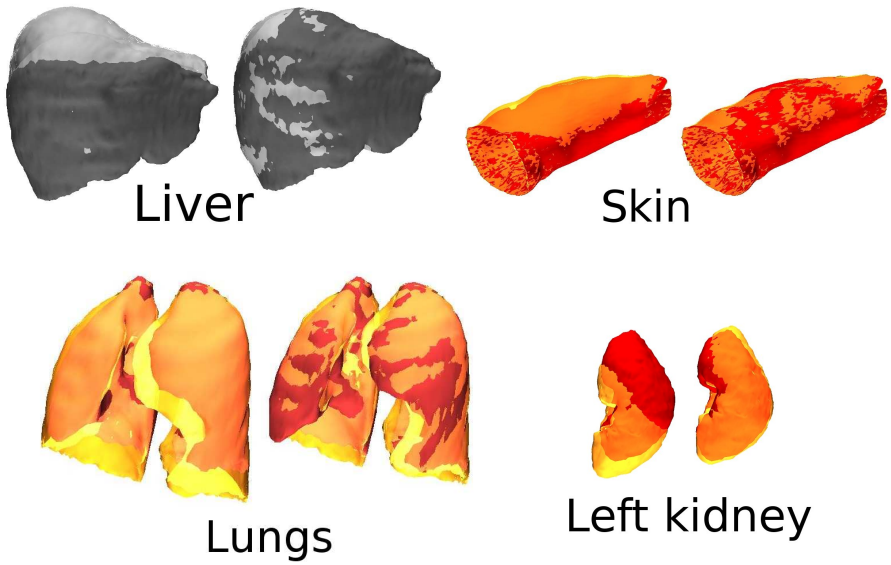

Fig. 6. Qualitative evaluation on organ meshes of our predicted simulation. For each organ: Left: in red: segmented meshes extracted from the expired CT acquisition. In Yellow: segmented meshes extracted from the inspired CT acquisition. Right: in red: segmented meshes extracted from the expired CT acquisition. In Yellow: segmented meshes simulated from the inspired CT acquisition.

5 Conclusion

In this paper we provide a new model to simulate and predict the movement of the internal organs due to breathing motion. Firstly, we showed that it is possible to estimate the displacement of any internal organ from a real time tracking of patient skin. Secondly, we proposed an original method to compute a deformation field from skin position that takes the physical properties of the internal organs into account (incompressibility of viscera, rib rotation, lung deformability). Finally, we evaluated our simulation model with CT-data of a volunteer and showed that our method is not only able to predict in real-time (14 Hz) internal organ motions, but also to provide a prediction accuracy within 7 mm. Since the observed errors have been measured on the organ boundaries, we are confident that our simulation model can provide a position prediction of a pathology inside an organ with an error under 4 mm.

Our current system uses data from a stereoscopic tracking system that require to stick several radio-opaque markers on the patient skin before the preoperative CT acquisition and during the intervention. We are aware that this is uncomfortable for both the patient and the practitioner. We are currently developing a structured light reconstruction system that will allow to avoid markers on skin and to use its full surfacic information.

In the coming months, we plan to provide a larger evaluation on a database of 10 voluntareers. Then, we will make a careful validation of the prediction accuracy on specific features of some organs (hepatic vessels for instance) using a tracked US probe as a control.

References

1. K. S. Arun, T. S. Huang, and S. D. Blostein. Least-squares fitting of two 3d point sets. *IEEE Trans. on PAMI*, 9(5):698–700, september 1987.
2. J.M. Balter, K.L. Lam, C.J. McGinn, T.S. Lawrence, and R.K. Ten Haken. Improvement of CT-based treatment-planning models of abdominals targets using static exhale imaging. *Int. J. Radiation Oncology Biol. Phys.*, 41(4):939–943, 1998.
3. L. Bornemann et al. OncoTREAT: A software assistant for oncological therapy monitoring. In *CARS*, pages 429–434, 2005.
4. M. Clifford et al. Assessment of hepatic motion secondary to respiration for computer assisted interventions. *Computer Aided Surgery*, 7:291–299, 2002.
5. S. Cotin, H. Delingette, and N. Ayache. A hybrid elastic model allowing real-time cutting, deformations and force-feedback for surgery training and simulation. *The Visual Computer*, 16(8):437–452, 2000.
6. M. Fiala. Artag, an improved marker system based on artoolkit. NRC/ERB-1111 NRC 47166, National Research Council Canada, July 2004.
7. Delingette H. Efficient linear elastic models of soft tissues for real-time surgery simulation. In *MMVR 7 (Medicine Meets Virtual Reality)*, pages 139–151, 1999.
8. Schwartz J.-M. Modelling liver tissue properties using a non-linear visco-elastic model for surgery simulation. *Medical Image Analysis*, 9(2):103–112, 2005.
9. Anonymous for the review.
10. S. Nicolau, X. Pennec, L. Soler, and N. Ayache. A complete augmented reality guidance system for liver punctures: First clinical evaluation. In *Proceedings MICCAI05*, page submitted, 2005.

11. V. Remouchamps et al. Significant reductions in heart and lung doses using deep inspiration breath hold with active breathing control and intensity-modulated radiation therapy for patients treated with locoregional breast irradiation. *Int. J. Radiation Oncology Biol. Phys.*, 55:392–406, 2003.
12. D. Sarrut et al. Simulation of 4d ct images from deformable registration between inhale and exhale breath-hold ct scans. *Medical physics*, 33(3):605–617, 2006.
13. T. Secomb. A theoretical model for the elastic properties of very soft tissues. *Biorheology*, 38(4):305–317, 2001.
14. L. Soler et al. Virtual reality and augmented reality in digestive surgery. In *IEEE ISMAR'04*, November 2004.
15. Kühnapfel U. Endoscopic surgery training using virtual reality and deformable tissue simulation. *Computer and Graphics*, 24(5):671–682, 2000.
16. F. Wacker et al. An augmented reality system for mr image-guided needle biopsy: Initial results in a swine model. *Radiology*, 238(2):497–504, February 2006.
17. J. Wong et al. The use of active breathing control (abc) to reduce margin for breathing motion. *Int. J. Radiation Oncology Biol. Phys.*, 44(4):911–919, 1999.